Theoretical and experimental study of two discrete coupled Nagumo chains

V. I. Nekorkin and V. B. Kazantsev
Radiophysical Department, Nizhny Novgorod State University, 23 Gagarin Avenue, 603600 Nizhny Novgorod, Russia

S. Morfu, J. M. Bilbault, and P. Marquié
Laboratoire LE2I, (FRE) CNRS 2309, Aile des Sciences de l'ingénieur, Université de Bourgogne, Boîte Postale 47870, 21078 Dijon Cedex, France

(Received 28 December 2000; revised manuscript received 12 April 2001; published 20 August 2001)

We analyze front wave (kink and antikink) propagation and pattern formation in a system composed of two coupled discrete Nagumo chains using analytical and numerical methods. In the case of homogeneous interaction among the chains, we show the possibility of the effective control on wave propagation. In addition, physical experiments on electrical chains confirm all theoretical behaviors.

DOI: 10.1103/PhysRevE.64.036602 PACS number(s): 45.05.+x

I. INTRODUCTION

In a variety of spatially extended systems arising in many areas of science, the competition between stationary states may yield the appearance of propagating front waves or kinks. These processes, defining the interfaces between different states of the medium, occur, for example, in some problems of cardiology, neurophysiology, chemistry, and physics (see, e.g., Refs. [1–3]). In particular, in a wide class of systems possessing front wave solutions, a significant place is taken by reaction-diffusion systems (RD systems). At present, among RD systems, the most deeply studied is the one-component Nagumo equation, which corresponds to the well-known FitzHugh-Nagumo system without the recovery variable. There are two cases of Nagumo equation considered in the literature, with respectively continuous and discrete spatial coordinates.

In the first case, this equation takes the form

$$u_t = d u_{xx} + F(u), \tag{1.1}$$

where $u(x,t)$ is the state variable, and d is the diffusion constant. The nonlinearity, providing the bistability of the medium, is expressed by $F(u) = -(u-m_1)(u-m_2)(u-m_3)$, with $0 < m_1 < m_2 < m_3$. It is well known (see, e.g., Refs. [4], [5]) that Eq. (1.1) has front wave or kink solutions of the form $u(x,t) = U(x-ct) \equiv U(\xi)$ with

$$U(\xi) \equiv \frac{m_3 + m_1 \exp\left(\pm \frac{m_3 - m_1}{\sqrt{2d}} \xi \right)}{1 + \exp\left(\frac{m_3 - m_1}{\sqrt{2d}} \xi \right)}, \tag{1.2}$$

and

$$c = \pm \sqrt{d/2}(m_1 + m_3 - 2m_2). \tag{1.3}$$

The signs $\pm$ correspond to kink and antikink solutions, respectively.

The discrete Nagumo equation has the form

$$\dot{u}_j = d(u_{j-1} - 2u_j + u_{j+1}) + F(u_j), \tag{1.4}$$

with the dot accounting for the time derivative, and j defining a space lattice point ($j \in \mathbf{Z}$) or discrete space coordinate, d being the coupling coefficient. Equation (1.4) is more preferable when the activity of the medium is provided by localized units in the junctions of the space lattice. Take, for instance, a myelinated nerve fiber [2], when the membrane activity is localized mostly in Ranvier nodes coupled by myelinated (passive) parts of the axon. Another example is the heart tissue composed of a number of interacting cardiac cells suitably distributed in space and coupled with gap junctions which may be approximated with nearest neighbor diffusive coupling [6,7]. From an engineering point of view, discrete RD systems, based on nonlinear electric RD lattices [8–11] or biological enzyme transistor circuits [12], can be used for various information processing problems.

Although Eq. (1.4) presents behavior qualitatively similar to Eq. (1.1), it also displays some different properties [13–22]. In particular, there exists a critical value of the coupling coefficient $d = d^*(m_1, m_2, m_3)$, above or under which front propagation is possible or not.

(i) For $d > d^*$, front wave solutions of two types (kinks and antikinks) are possible in Eq. (1.4), and do not differ qualitatively from solutions of Eq. (1.1).

(ii) For $d \leqslant d^*$, the propagation of front waves is impossible in Eq. (1.4) for any relations between parameters m_1, m_2, and m_3. This so called propagation failure phenomenon does not exist in the continuous case modeled by Eq. (1.1).

Figure 1 illustrates the dependence of front waves speed in Eq. (1.4) on parameter m_2, for a given d. In contrast with the continuous case depicted by Eq. (1.1) and shown by dashed curves in Fig. 1, there is an interval of m_2 in which $c = 0$, corresponding to the propagation failure. However, in many cases, one has to consider not only a single chain, but systems consisting of different interacting chains. For example, the sciatic nerve of animals consists of several hundred fibers, with some spatially distributed electric contacts. In this context, there is a growing interest devoted to the understanding of interfiber interactions [23–26].

The goal of this paper is to investigate the dynamics of a system composed of two coupled discrete chains modeling two coupled FitzHugh-Nagumo chains without recovery variables. Our system is expressed under the normalized forms

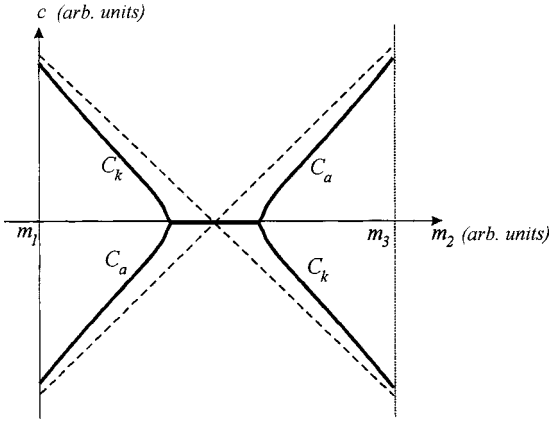

FIG. 1. Dependence of the velocity of possible front waves on parameter m_2 for $d=0.05$ in the chain [Eq. (1.4)] with $N=50$. The curve originating at $m_2=0$, with $c(m_2)>0$, corresponds to kinks, and with $c(m_2)<0$ to antikinks.

$$\dot{u}_j = f(u_j) + d(u_{j-1} - 2u_j + u_{j+1}) - h_j(u_j - v_j),$$

$$\dot{v}_j = f(v_j) + d(v_{j-1} - 2v_j + v_{j+1}) - h_j(v_j - u_j), \quad (1.5)$$

where the cubic function $f(w)$ is given by

$$f(w) = w(w-1)(a-w), \quad 0 < a < 1,$$

h_j and d, respectively, being the interchain and intrachain coupling coefficients [h_j is a vector with j defining a space chain point ($j=1,2,...,N$)]. However, for the sake of simplicity, we will restrict our study to the homogeneous interchain coupling case, that is, $h_j = h, \forall j$. Furthermore, we impose Neumann boundary conditions to system (1.5):

$$w_0 = w_1, \; w_{N+1} = w_N. \quad (1.6)$$

This paper is organized as follows. In Sec. II, we discuss the main properties of system (1.5) from a phase space point of view. In Sec. III, we inquire into the existence of patterns, high multistability, and wave propagation failure in system (1.5). Then, in Sec. IV, we study the dynamics of the system resulting in wave motions. Finally, experimental results on a real system composed of two coupled bistable electrical chains are presented in Sec. V.

II. MAIN PROPERTIES OF SYSTEM (1.5)

A. Confinement of trajectories

In this section we show that all trajectories of system (1.5) are confined. For this purpose, we introduce the r family of regions in phase space,

$$\Omega_r = \{u, v : -r \leqslant u_j \leqslant 1+r, -r \leqslant v_k \leqslant 1+r, \forall j,k = 1,2,...,N\},$$

with $r \geqslant 0$ being an arbitrary parameter. Let us consider the vector field of Eq. (1.5) at the boundaries of each of such regions. It follows from Eq. (1.5) that

$$\dot{u}_j\big|_{\{u_j=-r,\, -r\leqslant u_i\leqslant 1+r,\, i\neq j\}} = f(-r) + d(u_{j-1} + 2r + u_{j+1}) + hr + hv_j \geqslant f(-r) > 0,$$

$$\dot{u}_j\big|_{\{u_j=1+r,\, -r\leqslant u_i\leqslant 1+r,\, i\neq j\}} = f(1+r) + d(u_{j-1} - 2(1+r) + u_{j+1}) - h(1+r) + hv_j \leqslant f(1+r) < 0.$$

Similarly, we determine the orientation of v_j components on the boundary of Ω_r. This coincides with the orientation of the u_j components. Therefore, for $r>0$, the vector field of system (1.5) at the boundary of each Ω_r region is oriented inward. Hence all trajectories of system (1.5) with initial conditions outside Ω_0 come into this region as time proceeds, and do not leave Ω_0. Then, in the following, we consider the dynamics of system (1.5) in Ω_0. Note that the vector field at the boundary of Ω_0 is oriented inward everywhere excluding the two ''angle'' points $O_0(u_j=v_j=0)$ and $O_1(u_j=v_j=1)$, where $j=1,2,...,N$, which are the steady states of system (1.5). Then

$$0 \leqslant u_j \leqslant 1, \; 0 \leqslant v_k \leqslant 1 \quad \text{for } t>0, \; \forall j,k = 1,2,...,N. \quad (2.1)$$

B. Gradient property of the system

Let us consider the function

$$U = \sum_{j=1}^{N} \left[\frac{d}{2}(u_{j+1} - u_j)^2 + \frac{d}{2}(v_{j+1} - v_j)^2 - \int_0^{u_j} f(\eta)\, d\eta - \int_0^{v_j} f(\eta)\, d\eta + \frac{h}{2}(u_j - v_j)^2 \right]. \quad (2.2)$$

Using U, system (1.5) can be rewritten in the forms

$$\dot{u}_j = -\frac{\partial U}{\partial u_j}, \quad \dot{v}_j = -\frac{\partial U}{\partial v_j},$$

which show that Eq. (1.5) is a gradient system. Hence the attractors in the R^{2N} phase space can only be steady states of Eq. (1.5) [27]. Then any initial condition tends to one of the stable steady states corresponding to a local minimum of function U.

III. SPATIAL PATTERNS

In the ''physical'' space $\{(\mathbf{Z},\mathbf{R})\}$, each of the stable steady states defines a Turing-like pattern with a spatial profile corresponding to the distribution of the steady state coordinates. For example, steady states O_0 and O_1 correspond to stable homogeneous states of the medium. Let us find the maximum number of possible stable steady states, corresponding to steady patterns. For this purpose, we use the invariant domains technique (see Ref. [28] for details).

For convenience, we define the vector $w = (u_1, u_2, \ldots, u_N, v_1, v_2, \ldots, v_N)^T$, the superscript T denoting

the transpose operator, and the following regions in the phase space:

$$\Omega_i^0=\{w:\ 0\leqslant w_i\leqslant q,\ \ 0\leqslant w_k\leqslant 1,\ \ \forall k\neq i\},$$

$$\Omega_i^1=\{w:\ 1-p\leqslant w_i\leqslant 1,\ \ 0\leqslant w_k\leqslant 1,\ \ \forall k\neq i\},$$

with $0<q,p<1$. Let us show that, for parameter values taken from the region

$$D_{ch}=\begin{cases} 2d+h<\dfrac{a^2}{4} & \text{if } a\leqslant\dfrac{1}{2} \\ 2d+h<\dfrac{(1-a)^2}{4} & \text{if } a\geqslant\dfrac{1}{2}, \end{cases} \tag{3.1}$$

there exist p and q ensuring that the vector field of system (1.5) at the boundaries of each of these regions, Ω_i^0 and Ω_i^1, is oriented inward from them. For example, we consider the behavior of v_j components at the boundaries of Ω_i^0 and Ω_i^1. Taking Eq. (2.1) into account, we find

$$\begin{aligned}\dot v_j\big|_{\{v_j=q,0\leqslant w_k\leqslant 1,k\neq j\}}&=d(v_{j-1}-2q+v_{j+1})+f(q)-hq+hu_j\\ &\leqslant d(-2q+2)+f(q)-hq+h<0.\end{aligned} \tag{3.2}$$

Let us demand the negativeness of derivative (3.2). It is satisfied for any values of q obeying

$$\frac{a}{2}-\left(\frac{a^2}{4}-2d-h\right)^{1/2}<q<\frac{a}{2}+\left(\frac{a^2}{4}-2d-h\right)^{1/2}. \tag{3.3}$$

Similarly, at the boundary of region Ω_i^1, we find

$$\begin{aligned}\dot v_j\big|_{\{v_j=1-p,0\leqslant w_k\leqslant 1,k\neq j\}}&=d(v_{j-1}-2(1-p)+v_{j+1})\\ &\quad+f(1-p)-h(1-p)+hu_j\\ &\geqslant -2d(1-p)+f(1-p)-h(1-p)\\ &>0.\end{aligned} \tag{3.4}$$

The values of parameter p ensuring the positiveness of derivative (3.4) are defined by

$$\begin{aligned}&\frac{1-a}{2}-\left(\frac{(1-a)^2}{4}-2d-h\right)^{1/2}\\ &\qquad<p<\frac{1-a}{2}+\left(\frac{(1-a)^2}{4}-2d-h\right)^{1/2}.\end{aligned} \tag{3.5}$$

In the same manner, we determine the orientation of components u_j at boundary planes $\{u_j=q\}$ and $\{u_j=1-p\}$ of regions Ω_j^0 and Ω_j^1. By construction, the boundary of each of the regions Ω_j^0 consists of two parts, one of them formed by planes $\{w_j=q\}$ and the other one by the boundary of region Ω_0 (see Sec. II). Therefore, at the boundary of each of regions Ω_j^0, the vector field of system (1.5) is oriented inward. Similarly, we obtain that trajectories of Eq. (1.5) intersect the boundaries of regions Ω_j^1 inward. Let us fix an arbitrary

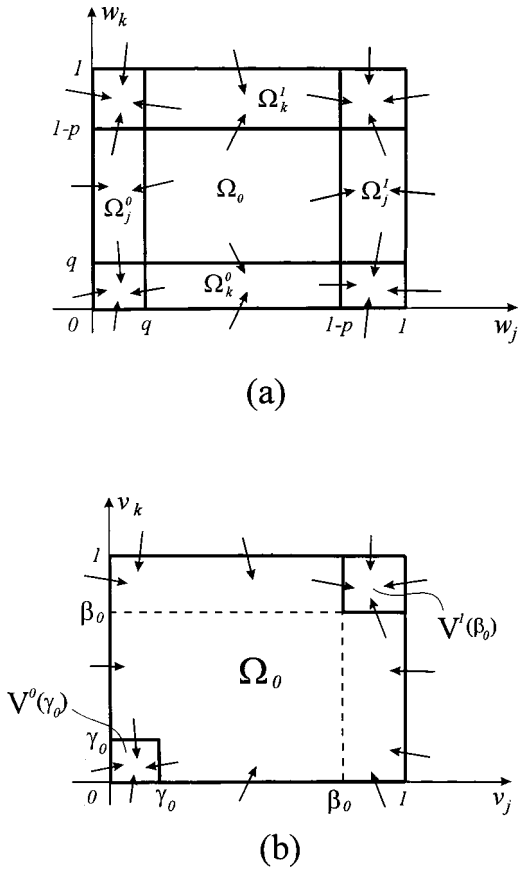

FIG. 2. (a) Qualitative representation of the J set. (b) Qualitative representation of regions $V^0(\gamma_0)$ and $V^1(\beta_0)$.

sequence of length N composed of two symbols $a_j\in\{0;1\}$, and consider the intersection $J=\cap\Omega_j^{a_j}$ [see Fig. 2(a)]. J being represented by the direct product of the segments of the coordinate axes, it is a convex compact set. In addition, the boundary of J is formed by the boundaries of regions Ω_j^0 and Ω_j^1; hence the trajectories of system (1.5) intersect this boundary inward from region J. Obviously, set J contains at least one attractor of system (1.5). Using the gradient property of the system, we find that this attractor can be represented only by a steady state. Since there are 2^N sets or J-type regions, there exist 2^N stable steady states in the phase space of system (1.5).

Thus system (1.5) displays a high multistability. Since the steady states can be encoded by arbitrary sequences of two symbols, the possible pattern profiles in $\{\mathbf{Z},\mathbf{R}\}$ are extremely diverse, varying from regular to complex disordered configurations. For illustration, we may obtain a disordered pattern on u components and a regular one on v components, as shown in Fig. 3. Note that the existence of a wealth of steady patterns does not allow any wavelike motion in system (1.5). In fact, the origin of wave propagation failure, quite typical in discrete bistable systems, lies in the existence and stability of patterns: the regions $\Omega_j^i(i\in\{0,1\})$ estimate the steady state attraction basins. Their initial conditions belonging to one of these regions, kinks or antikinks, are attracted by the corresponding steady state. Thus the parameter values taken in region D_{ch} give sufficient conditions to observe this phenomenon.

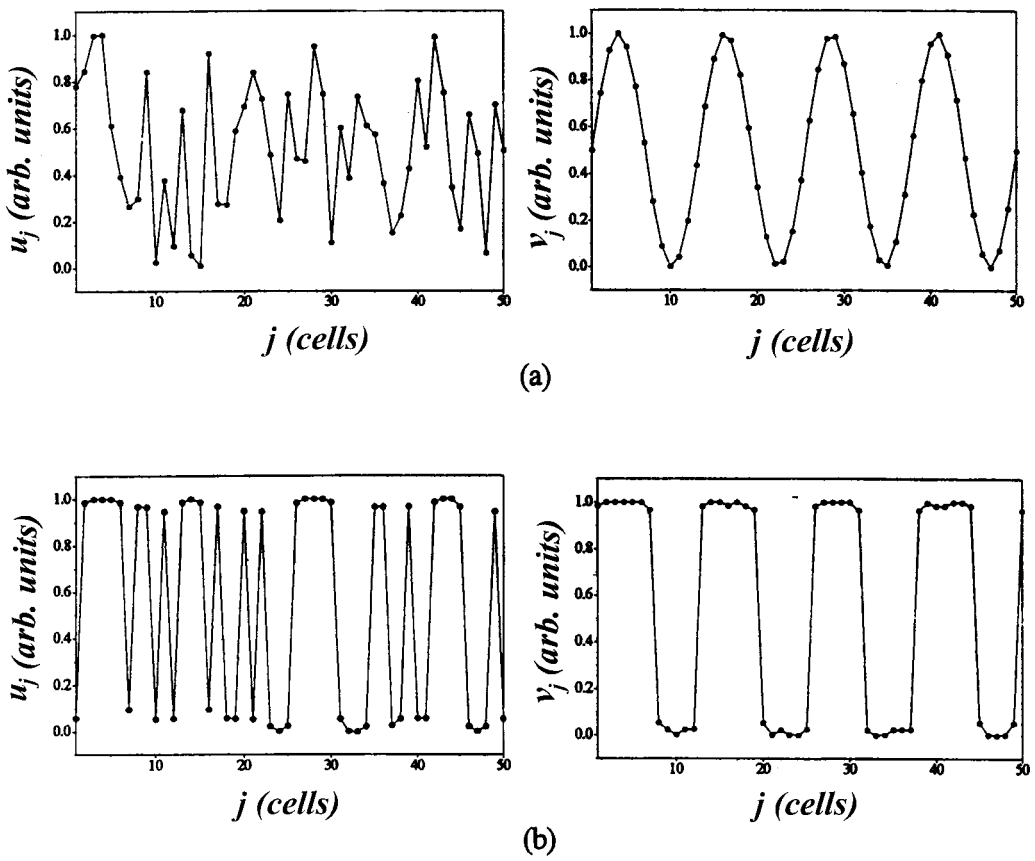

FIG. 3. Formation of steady patterns in both coupled chains described by system (1.5). (a) Initial conditions. (b) Terminal patterns. Parameter values: $a=0.4$, $d=0.01$, and $h=0.01$ (arbitrary units).

IV. TRAVELING WAVES

For illustration, in this section we treat system (1.5) as two coupled chains divided in real space. First, we note that the results of Ref. [29] ensure the complete interchain synchronization of all motions for strong enough interchain coupling

$$h_j > \frac{a^2-a+1}{6}. \tag{4.1}$$

Then, in the R^N phase space of system (1.5), there is an N-dimensional (synchronization) manifold which attracts all motions. In this manifold, motions are governed by a system of like Eq. (1.4), with $F(u) \equiv f(u)$. In this case, the traveling wave dynamics does not depend on the coefficients h, and is illustrated by Fig. 1. We will now consider the dynamics of the system for small enough interchain interaction.

A. Front waves, slowing down, stopping, and about turn

Let us consider a front wave or kink propagating in the first chain (u components), while the second chain (v components) is in the vicinity of the homogeneous steady state O_0. For convenience, we call this state ''unexcited,'' because all elements have coordinates close to zero. We switch on the interaction, and analyze how small but nonzero coupling acts on the propagating front.

Let us introduce the following γ family of regions in phase space:

$$V^0(\gamma) = \{u,v : 0 \leqslant v_j \leqslant \gamma, 0 \leqslant u_k \leqslant 1, \forall j,k = 1,2,...,N\}.$$

Then there exist such values of γ for which the trajectories of system (1.5) intersect the boundary of $V^0(\gamma)$ inward from this region. Indeed, it is satisfied at the parts of $V^0(\gamma)$ inherited from region Ω_0 [see Sec. II and Fig. 2(b)]. Considering the rest part of $V^0(\gamma)$ and using Eq. (2.1), we obtain, from Eq. (1.5),

$$\begin{aligned} \dot{v}_j|_{\{v_j=\gamma, 0\leqslant v_k\leqslant\gamma, k\neq j, 0\leqslant u_j\leqslant 1\}} &= f(\gamma) + d(v_{j-1} - 2\gamma + v_{j+1}) - h\gamma + hu_j \\ &\leqslant f(\gamma) - h\gamma + h. \end{aligned} \tag{4.2}$$

The negativeness of derivative (4.2) is fulfilled for

$$\gamma_0 \equiv \frac{a}{2} - \left(\frac{a^2}{4} - h\right)^{1/2} < \gamma < \frac{a}{2} + \left(\frac{a^2}{4} - h\right)^{1/2} \tag{4.3}$$

Hence for Eq. (4.3) the vector field of Eq. (1.5) is oriented inward from these regions. Then, if the initial conditions in system (1.5) are taken inside $V^0(\gamma_0)$, the corresponding trajectory satisfies

$$0 \leqslant v_j \leqslant \gamma_0, \quad 0 \leqslant u_k \leqslant 1, \quad \text{for } t>0, \quad \forall j,k=1,2,...,N. \tag{4.4}$$

Since $\gamma_0 < a/2$, conditions (4.4) mean that components v_j, for any $t>0$, stay below the ''excitation threshold'' (the definition of the ''unexcited'' chain) and components u_j may take arbitrary values within the region Ω_0.

Introducing a fixed positive parameter ε with an infinitely small value, it is easy to show that for

$$h \leqslant a\varepsilon + O(\varepsilon^2), \tag{4.5}$$

the parameter γ_0 satisfies the inequality $\gamma_0 \leqslant \varepsilon$. In this case, motions in the second chain are on the order of an infinitely small value; hence the chain evolves in the vicinity of its steady state O_0. In spite of the smallness of h, expressed in Eq. (4.5), the dynamics of the first chain becomes quite different. Indeed, in this case,

$$h(u_j - v_j) = hu_j + O(\varepsilon^2). \tag{4.6}$$

Then, in a first order approximation on ε, the dynamics of the first chain is defined by system (1.4) with $F(u)=f(u)-hu$. The zeros of $F(u)$ are given by

$$m_1 = 0, \quad m_{2,3} = \frac{1+a}{2} \mp \left(\frac{(1-a)^2}{4} - h \right)^{1/2}. \tag{4.7}$$

Thus, in the case of weak interchain coupling, the second chain stays in its ''unexcited'' state, while the first chain supports the front propagation with a new velocity. Indeed, according to Eq. (4.7), we obtain

$$m_2(h) > m_2(0) = a. \tag{4.8}$$

Since the kink velocity is a monotonically decreasing function of parameter m_2 (Fig. 1), the influence of the second chain, $h>0$, tends to decrease the velocity of the kink in chain 1. Analyzing the diagram in Fig. 1 leads to the following possibilities concerning the dynamics of the kink: (*a*) *the kink is propagating with a smaller velocity*, $c(h)<c(0)$; (*b*) *the kink stops to propagate*, $c(h)=0$; and (*c*) *the kink reverses and propagates backward*, $c(h)<0$. Such behaviors of the kink have been verified in numerical simulations of system (1.5). For example, the velocity-coupling dependence $c=c(h)$, obtained for $a=0.45$ and shown in Fig. 4, involves the three possibilities successively. For comparison, corresponding curves obtained with the first-order perturbation analysis [Eqs. (4.5)–(4.7)] are shown by dashed lines. There is a good qualitative (and quantitative for $h \to 0$) agreement with direct simulation of system (1.5). Case (a), realized for smallest values of h, is illustrated in Fig. 5. The front propagating in the first chain for $h=0$ with a definite velocity becomes slower when switching on the interaction at $t=t_0$. This corresponds to the different angle shown in the space-time plot (j,t) in Fig. 5. The second chain remains ''unexcited.'' The front stops with increasing h. Hence the stopping front results in a ''kinklike'' steady pattern in the propagation failure. In contrast to the description of Sec. III, the origin of this phenomenon is not caused by internal dynamics for small d, but by the interchain dynamics with nonvanishing h. A further increase of h leads to the kink reversing, as shown in Fig. 6. Finally, the break of the velocity curves in Fig. 4

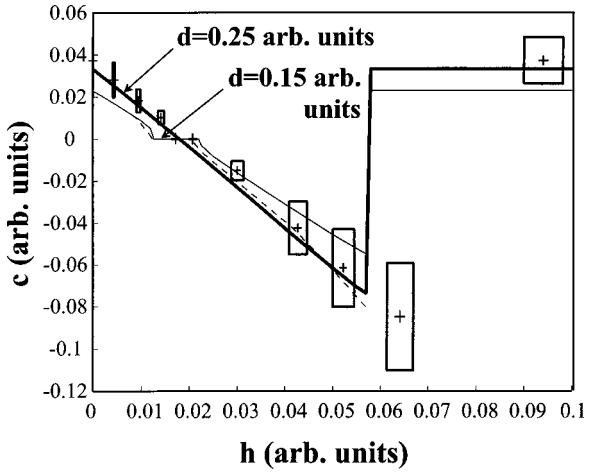

FIG. 4. Velocity-coupling dependences (solid curves) for a kink interacting with an ''unexcited'' state in the second chain. Parameter values: $N=50$ and $a=0.45$. The dashed curve shows the dependence $c(h)$ obtained with the perturbation analysis [Eqs. (4.5)–(4.7)] for $d=0.15$. The solid lines represent numerical simulation with $d=0.15$, and 0.25 (bold line). Experimental results are represented by crosses in the case $d=0.25\pm0.02$.

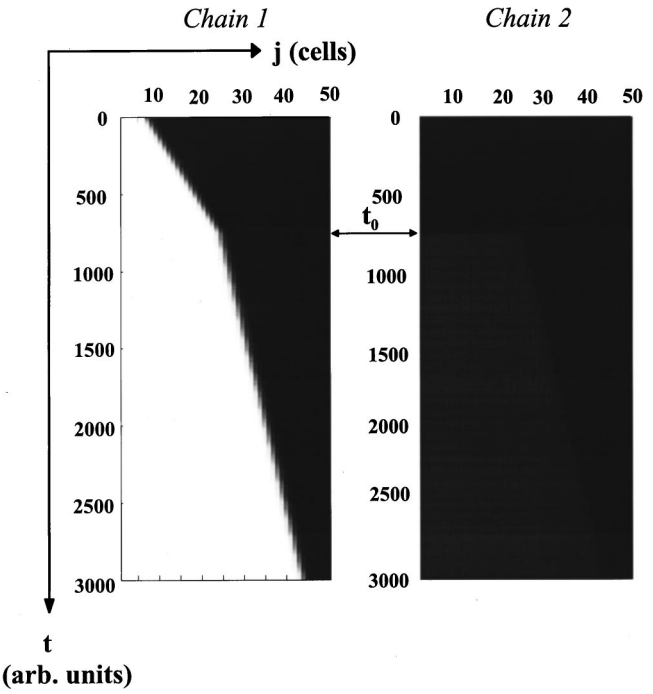

FIG. 5. Space-time plot of kink propagation in system (1.5). The interchain interaction is switched on at a time instant t_0. The dynamics of the u_j and v_j components is shown by the levels of gray (the scale is not shown) with white corresponding to the ''excited'' state, and black to the ''unexcited'' state. The kink corresponds to the white-black interface. The light gray in the right-hand picture shows the small perturbation of the second chain. Parameter values: $N=50$, $a=0.45$, $d=0.15$, and $h=0.01$.

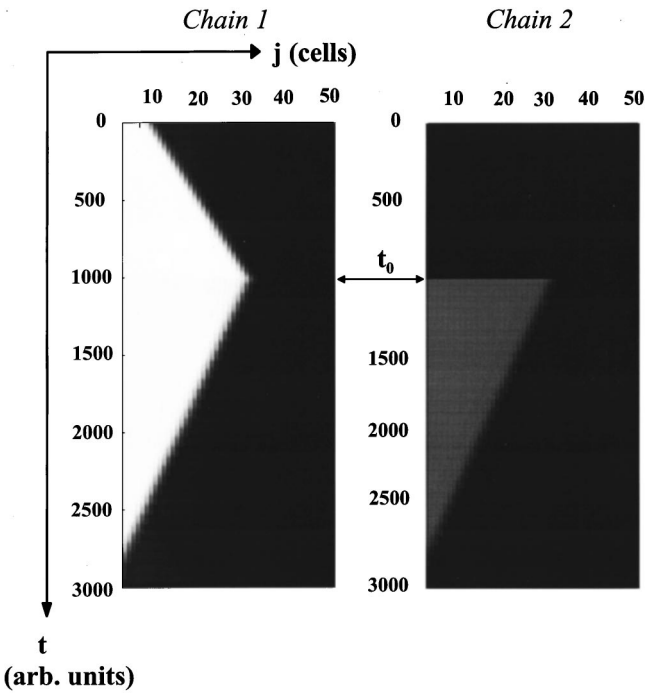

FIG. 6. Kink reversing in system (1.5). Parameter values: $N=50$, $a=0.45$, $d=0.15$, and $h=0.03$.

corresponds to interchain synchronization, that is, the second chain displays a kink identical to the original. As mentioned earlier, the dynamics in this case is defined by the equations for a single chain [Eq. (1.4)]; hence the velocity of both synchronized kinks is equal to the unperturbed case $h=0$.

Note that the increase of intrachain coupling d tends to decrease the domain of zero velocities (Fig. 4). In the limit case of a continuous medium, described by partial differential equations (1.1), that is for $d \gg 1$, we may expect only one point with $c=0$.

B. Front waves speeding up

Let us now consider a front wave or kink propagating in the first chain (u components), while the second chain (v components) is in the vicinity of the homogeneous steady state O_1. We refer to this state as an ''excited'' one, because all elements have a coordinate close to 1. Considering the weak homogeneous interaction ($h>0$) between the two chains with such initial conditions, and processing as for the previous case, one can show that, for $h>[(1-a)^2/4]$, there is a region in the R^{2N} phase space which cannot be left by the trajectories of system (1.5). It has the form [see Fig. 2(b)]

$$V^1(\beta_0)=\{u,v:\ \beta_0 \leqslant v_j \leqslant 1, 0 \leqslant u_k \leqslant 1,\ \forall j,k=1,2,...,N\},$$

with

$$\beta_0 \equiv \frac{1+a}{2}+\left(\frac{(1-a)^2}{4}-h\right)^{1/2}.$$

Thus, for trajectories with initial conditions taken in region $V^1(\beta_0)$, we obtain the restriction

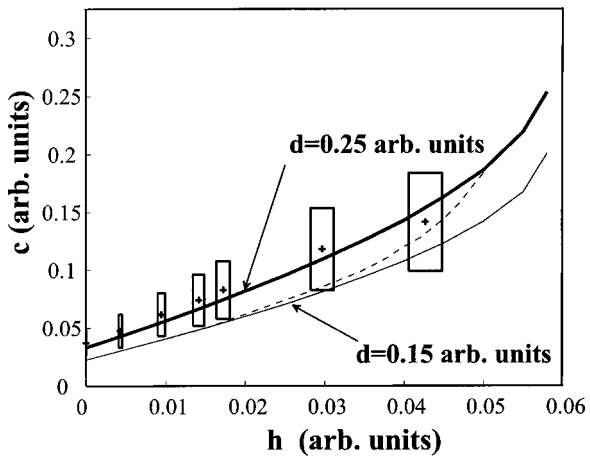

FIG. 7. Velocity-coupling dependences (solid curves) for the kink in chain 1, interacting with ''excited'' state in the second chain. The dashed curve shows the dependence $c(h)$ obtained with the perturbation analysis [Eqs. (4.11) and (4.12)], with $d=0.15$. Other parameter values are $N=50$ and $a=0.45$. The solid lines represent numerical simulations with $d=0.15$ and 0.25 (bold line). Experimental results are represented by crosses in the case $d=0.25 \pm 0.02$.

$$\beta_0 \leqslant v_j \leqslant 1, 0 \leqslant u_k \leqslant 1, \quad \text{for } t>0, \quad \forall j,k=1,2,...,N. \tag{4.9}$$

Since $\beta_0 > a$, such a state of the second chain can be considered as ''excited,'' in the sense that all v_j components have large enough values (in the vicinity of steady state O_1).

Let us fix an arbitrary infinitely small ε such that

$$1-\beta_0 < \varepsilon$$

and

$$h \leqslant (1-a)\varepsilon + O(\varepsilon^2). \tag{4.10}$$

From Eq. (4.10), we obtain

$$h(v_j-u_j) = -hu_j + h + O(\varepsilon^2). \tag{4.11}$$

With an accuracy up to ε^2, the dynamics of the first chain in Eq. (1.5) is defined by the single chain system [Eq. (1.4)] with $F(u)=f(u)-hu+h$ and parameters

$$m_{1,2}=\frac{a}{2} \mp \left(\frac{a^2}{4}-h\right)^{1/2}, \quad m_3=1. \tag{4.12}$$

Hence the function $m_2(h)$ is monotonically decreasing. Similarly to Eq. (4.7) discussed in Sec. IV A, and using Eq. (4.12), we find the following behavior. (*d*) *the kink traveling in the first chain has a greater velocity due to the interchain interaction,* $c(h)>c(0)$. The velocity-coupling dependence for a kink with increased velocity is shown in Fig. 7. The solid curves ($d=0.15$ and 0.25) was obtained from a direct simulation of Eq. (1.5) and the dashed one ($d=0.15$) from the perturbation approach using Eqs. (4.11), (4.12), and (1.4). For $d=0.15$, one can find very fine qualitative and quantitative agreements between these curves for small enough h,

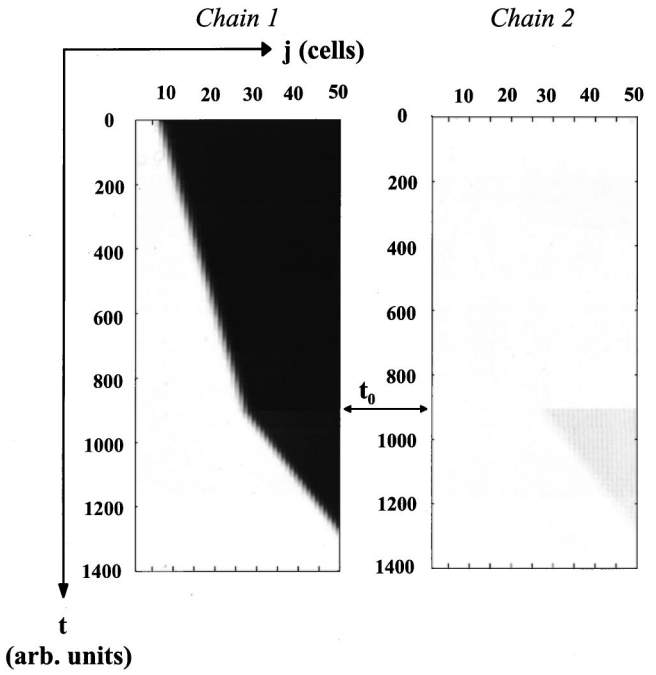

FIG. 8. Kink speeding up in the result of interaction with the ''excited'' state in chain 2. Parameter values: $N=50$, $a=0.45$, $d=0.15$, and $h=0.02$.

when the perturbation analysis is applicable. Note that the velocity curve ends up at some value of h. Similar to the break of the curves in Fig. 4, this corresponds to an interchain synchronization. In contrast with the synchronized kinks, the terminal state here is the ''excited'' state of both chains, i.e., the kink disappears as a result of synchronization. Figure 8 illustrates such a kink, whose velocity is increased, by switching on the interaction at t_0. Note that the dynamics of antikinks in system (1.5) is the ''opposite'' of that described for the kinks. For example, if the kink velocity increases when interacting with the ''excited'' chain, the antikink, if initially excited in the first chain, slows down or reverses with properties (a)–(c). If the antikink interacts with the ''unexcited'' state, its velocity increases with property (d). Using the symmetry property of function $f(u)$, the velocity-coupling dependences for the antikink propagation can be easily derived from diagrams of Figs. 4 and 7 by substituting $a \rightarrow 1-a$.

C. Fronts traveling along steady patterns

Let us suppose there is kink propagation in the first chain, while a steady pattern exists in the second. This situation may occur if the intrachain coupling coefficients are different. In particular, $d_1(a)$ is taken to provide the propagation, $c(a)>0$ in Fig. 1(c), and $d_2(a)$ is taken inside D_{ch} satisfying inequality (3.1) (Sec. III) with $h=0$. For simplicity, from a wealth of possible configurations, we take a periodic steady pattern with quite a large spatial scale, as shown in Fig. 3(b) (right picture). Then, using Eqs. (3.3) and (3.5), the coordinate elements are grouped in small neighborhoods near the ''excited'' (O_1) and ''unexcited'' (O_0) states of the second chain. Using the results of Secs. IV A and IV B, we may

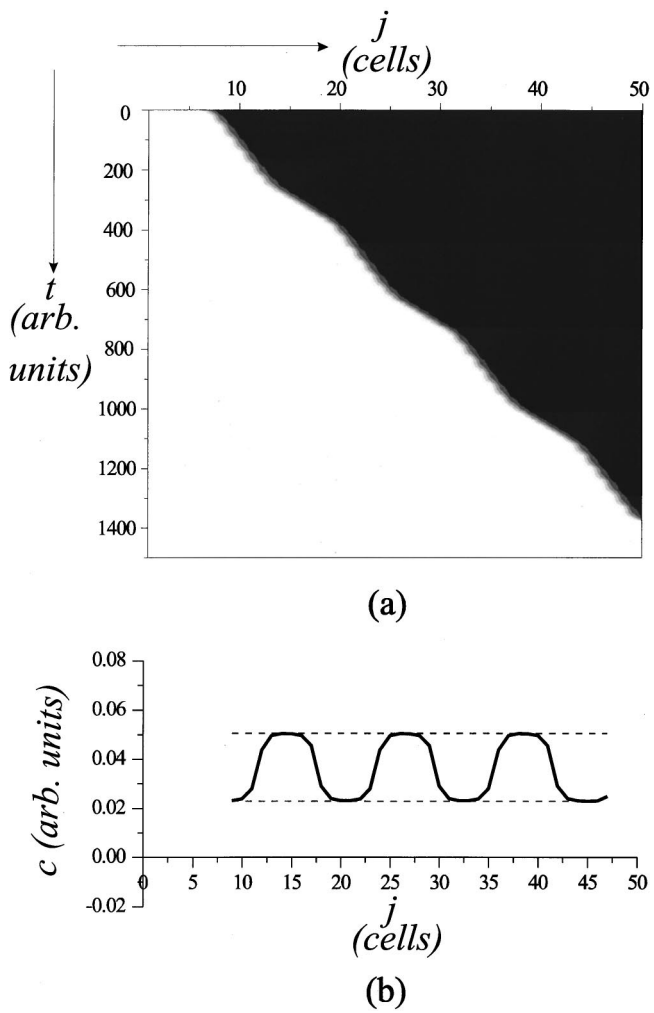

FIG. 9. Kink propagating along a steady periodic pattern in the second chain [Fig. 3(b), right picture]. (a) Modulation of the kink velocity in a space-time plot (j,t) for chain 1. (b) Instantaneous velocity $c_i(j)=1/\tau_j$, where τ_j is the time of the front to come from the $(j-1)$th to the jth elements, during the propagation. Dashed curves correspond to the homogeneous states O_1 (upper line) and O_0 (lower line) in the second chain. Parameter values: $N=50$, $a=0.4$, $d_1=0.1$, $d_2=0.01$, and $h=0.01$.

expect that, for certain values of $h \neq 0$, the kink in the first chain would slow down while traveling along the ''unexcited'' elements, and speed up when passing the excited elements. This has been verified numerically. We have calculated the instant velocity of the kink during the propagation. Its behavior is shown in Figs. 9(a) and 9(b). The velocity oscillates according to the profile of the steady pattern. The maximum and minimum limit velocity values are defined from the interaction of the kink with the excited and unexcited chains, respectively, and shown by dashed lines in Fig. 9(b).

V. FRONTS IN ELECTRONIC EXPERIMENTS

A. Experimental setup

Our experiments were carried out on two coupled identical electrical chains. Each of them is composed of $N=22$

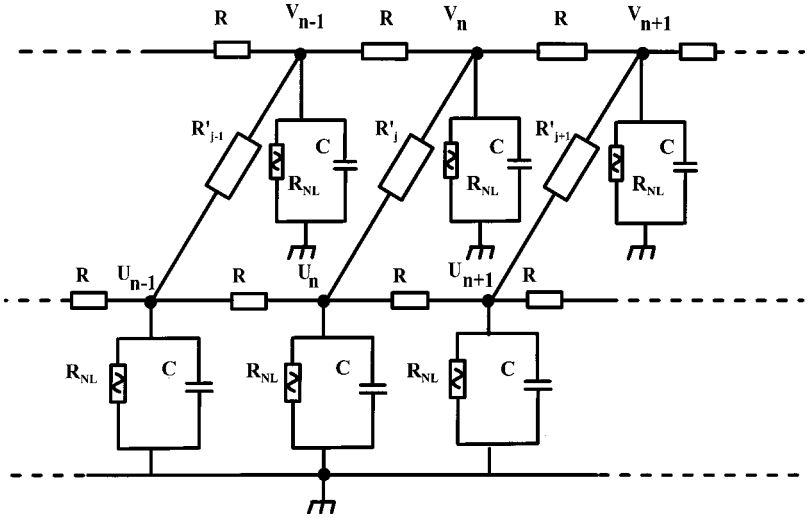

FIG. 10. Sketch of the experimental coupled electrical lattice.

cells (see Fig. 10), including a linear capacitance C and a nonlinear resistor R_{NL}, whose current-voltage characteristic obey the cubic function

$$I_{\mathrm{NL}}=\frac{V}{R_0}\times\left(1-\frac{V}{\alpha}\right)\times\left(1-\frac{V}{\beta}\right).$$

Here α and β are the roots of the characteristic, and R_0 is a weighting resistor. Intrachain diffusion coupling is assured by linear resistors R, while interchain diffusion coupling between cells repered by the same number j is assured by linear resistors R'. Using Kirchhoff laws, we can model the voltages evolutions, namely U_j in chain 1 and V_j in chain 2, by a set of coupled discrete equations:

$$\frac{dU_j}{dt}=\frac{1}{RC}(U_{j+1}+U_{j-1}-2U_j)-\frac{U_j}{R_0C}\left(1-\frac{U_j}{\alpha}\right)\left(1-\frac{U_j}{\beta}\right)-\frac{1}{R'C}(U_j-V_j),$$

$$\frac{dV_j}{dt}=\frac{1}{RC}(V_{j+1}+V_{j-1}-2V_j)-\frac{V_j}{R_0C}\left(1-\frac{V_j}{\alpha}\right)\left(1-\frac{V_j}{\beta}\right)-\frac{1}{R'C}(V_j-U_j). \tag{5.1}$$

In addition, the two chains satisfy Neumann boundary conditions. After normalization, namely setting $u_j=U_j/\beta$, $v_j=V_j/\beta$, $d=R_0(\alpha/\beta R_1)$, and $h=R_0(\alpha/\beta R')$, Eqs. (5.1) appear to be an analog simulation of system (1.5).

The state of the system is visualized in a video line, that is, every 64 μs, the voltage of each cell of chains 1 and 2 is collected as an analog luminance signal, where black corresponds to the state close to $V=0$ (the unexcited state) and white corresponds to the state close to $V=\beta$ (the excited state). These definitions were stated in Sec. IV. Using a parallel to serial converter, the resulting serial video output is then mixed with video synchronization, allowing us to visualize the resulting composite video on a monitor. Therefore, its screen will show the evolution of each cell of both chains vertically, with the time growing toward the bottom, such as the whole height corresponds to a local process time of 20 ms. For a detailed description of the experimental setup and initial data loading, see Ref. [11].

B. Observation of steady states

In order to check the theoretical predictions of Sec. III, summarized in Fig. 3, the components are chosen such as $R=100\,\mathrm{k}\Omega$, $R'=330\,\mathrm{k}\Omega$, $C=3.3\,\mathrm{nF}$, $\alpha=0.64\,\mathrm{V}$, and $\beta=1.45\,\mathrm{V}$. Therefore, $R_0=3.2\,\mathrm{k}\Omega$, and the parameters appearing in system (1.5) are fixed to be $d=0.014$, $h_j=h=0.004$, and $a=\alpha/\beta=0.44$. Note that these parameters verify condition (3.1). The initial conditions, loaded in the two chains, consist of arbitrary sequences of voltages between 0 and β, that is 0 and 1, respectively, after normalization. From initial conditions shown in Fig. 11(a), the real system evolves versus time, and gives final voltage profiles, as shown in Fig. 11(b), revealing that a steady state is reached for each lattice. These figures confirm that final voltages of every cell of both chain belong to regions Ω_i^0 or Ω_i^1 (see Sec. III and Fig. 3).

C. Front waves slowing down, stopping, and reversing

In this section, we intend to check experimentally the theoretical predictions of Sec. IV A. The electrical components keep the previous values, except C, which is now 10 nF, and intracoupling resistors R, now set to 5.6 kΩ; then $d=0.25$. In addition, the resistor R' will act as a parameter controlling the interchain coupling coefficient h. We first consider the case without interchain coupling, that is $h=0$, and study the propagation of a kink in the first chain, starting from initial conditions where the voltage of the six first cells of chain 1 corresponds to the excited state (white). The voltage of all other cells, including the cells of chain 2, corresponds to the unexcited state (black). The correspondent screens (see Fig. 12) show then a propagating front from left to right on the first chain, while nothing occurs in the second chain; that is, the voltages of every cell of chain 2 remain in the unexcited state. Note that the chains components values lead for both

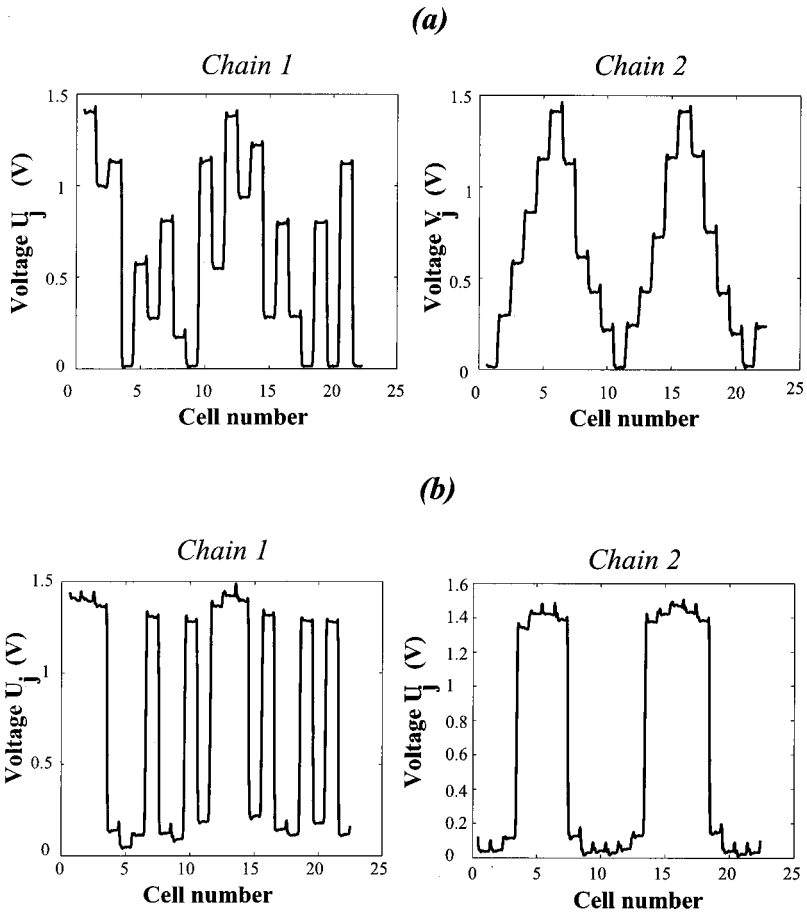

FIG. 11. Steady states or spatial patterns on both coupled chains: (a) initial condition, and (b) final state. Parameter values after normalization are $a=0.44\pm0.01$, $h=0.0043\pm0.0003$, and $d=0.014\pm0.001$ (all in arbitrary units), while $C=3.3$ nF.

lattices to an intrachain coupling coefficient d slightly larger than d^*, the critical value of propagation failure, whose estimation is given by inequalities (3.1) with $h=0$.

First, for small value of h (see Fig. 13, with $h=0.0043$), the kink velocity in the first chain becomes lower than in the case without intercoupling, that is $h=0$ (Fig. 12), while the behavior of the second chain seems to be unaffected. A comparison between Figs. 13 and 5 shows a good agreement

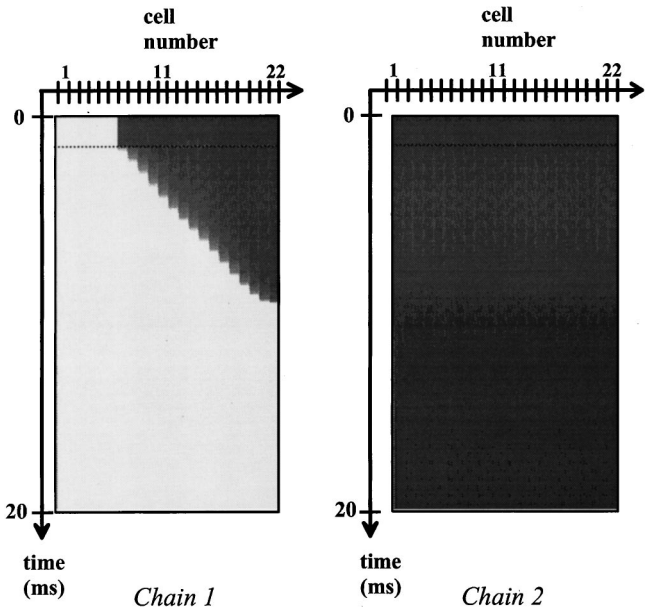

FIG. 12. Kink propagation on the first chain without interchain coupling. The second chain is in unexcited state. $a=0.45\pm0.01$, $h=0$, $d=0.25\pm0.02$, and $C=10$ nF.

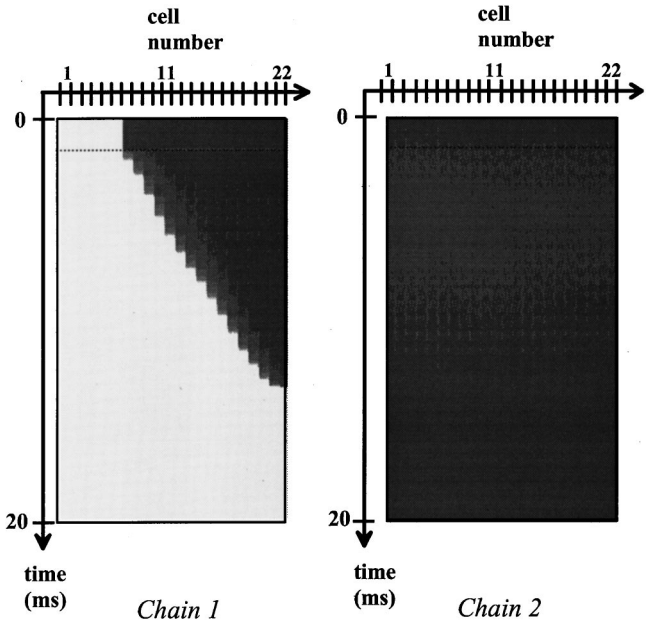

FIG. 13. The kink velocity decreases in the first lattice; the second one stays in an unexcited state. $a=0.45\pm0.01$, $h=0.0043\pm0.0002$, $d=0.25\pm0.02$, and $C=10$ nF.

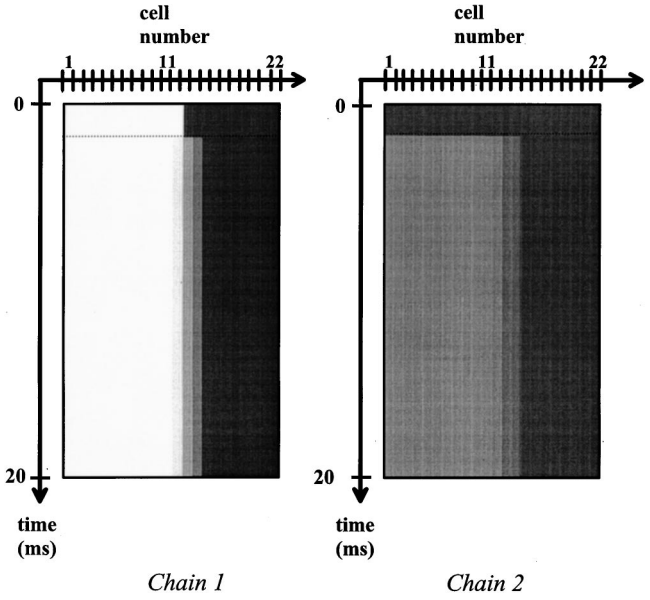

FIG. 14. Stop propagation of kink for $a=0.45\pm0.01$, $h=0.022\pm0.002$, $d=0.25\pm0.02$, and $C=10$ nF.

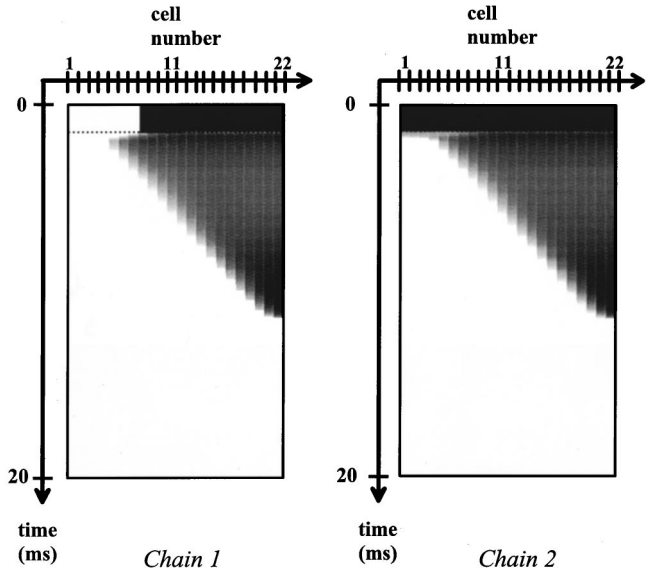

FIG. 16. Instantaneous synchronization of kinks in both lattices for $a=0.45\pm0.01$, $h=0.094\pm0.005$, $d=0.25\pm0.02$, and $C=10$ nF.

between theoretical and experimental behaviors. Now increasing h, we obtain the screens of Fig. 14, where the front wave is stopped in chain 1, while cell voltages in chain 2 stay very close to zero, that is in the unexcited state [see region $V^0(\gamma_0)$ in Fig. 2(b)]. For larger values of h, Fig. 15 shows an about turn of the front wave propagating in chain 1, that is, it now propagates backwards; however, cells of chain 2 still stay in region $V^0(\gamma_0)$ also [see Figs. 2(b) and 6]. Finally, for larger values of h, as represented in Fig. 16, a kink arises in chain 2, synchronized with the kink of chain 1.

All these experimental results are summarized in Fig. 4, and can be compared with the simulation predictions (continuous line) previously given. One can observe the qualitatively similar behavior between experimental results and simulation predictions. Note, however, that for practical reasons the following hold

(i) Quantitatively, the experimental crosses of Fig. 4 are not exactly superimposable on the simulation curve, because of different experimental defects: uncertainties in component values, and the current-voltage characteristic of R_{NL}, which differs from the cubic law. For these reasons, the crosses do not exactly agree with the simulation predictions (solid curve) for $d=0.25$; in particular, they show a zero-velocity part as predicted theoretically in Fig. 4 for smaller values of $d(d=0.15)$. This discrepancy can be mainly imputed to un-

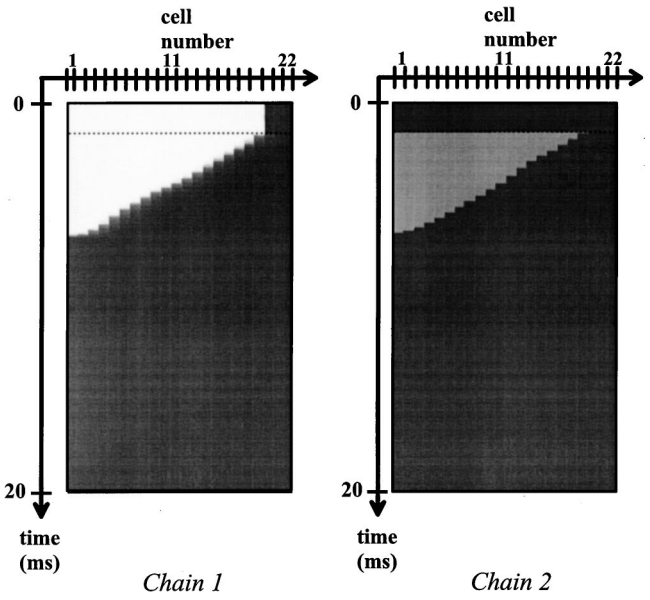

FIG. 15. The kink velocity becomes negative when $a=0.45\pm0.01$, $h=0.043\pm0.002$, $d=0.25\pm0.02$, and $C=10$ nF.

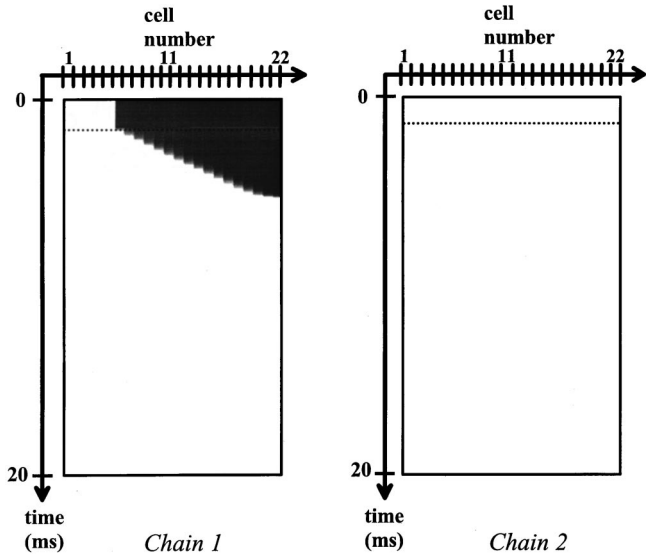

FIG. 17. When the second chain is initially in an excited state, the velocity of the wave front in the first chain is increased for $h\neq0$. Parameters values: $a=0.45\pm0.01$, $h=0.014\pm0.001$, $d=0.25\pm0.02$, and $C=10$ nF.

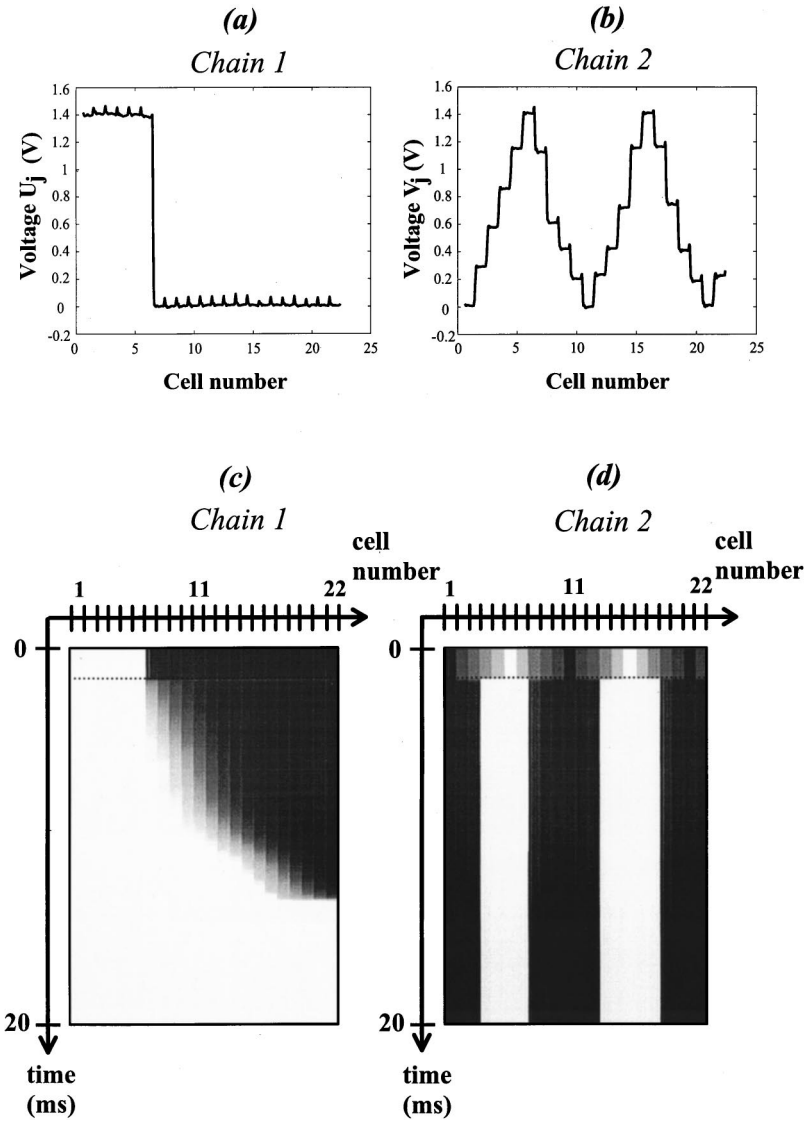

FIG. 18. Velocity modulation of a kink in chain 1. Starting from initial conditions (a) and (b), the kink on chain 1 undergoes velocity fluctuations (c) related to the steady state pattern existing in chain 2 (d). $a=0.44\pm0.01$, $h=0.0043\pm0.0003$, $d_1=0.43\pm0.03$, $d_2=0.0094\pm0.0008$, and $C=10$ nF.

certainties concerning the intrachain coupling coefficient d.

(ii) Experimentally, we cannot change all resistors R' for all cells at the same time t_0, as it is possible in simulations (see Figs. 5 and 6). Thus the video screens of Figs. 12, 13, 14, 15, and 16, only start after t_0.

However, the agreement between the theoretical behavior, for $t>t_0$, and the experimental one is quite satisfactory. In addition, the main features concerning the behavior of the system—that is stopping, about turn, and synchronization of front waves when the intracoupling h increases—correspond to theoretical predictions.

D. Front waves speeding up

This part is devoted to experimental investigations related to Sec. IV B. The parameters of the system are the same as in Sec. V C, that is, $a=0.45$, $R_0=3.2\,\mathrm{k}\Omega$, $C=10$ nF, and $d=0.25$. Decreasing resistors R' step by step, we control the intercoupling parameter h, and measure its effects on the kink propagation. That is, initial conditions are set as following (see Fig. 17, where $h=0.014$ for example): for chain 1, the five first cells are in the excited state 1 (white), while the others are in the unexcited state (black); for chain 2, all cells are in the excited state, so they belong to region $V^1(\beta_0)$ in Fig. 2(b). As the time increases, Fig. 17 shows that the kink now propagates faster in chain 1, with respect to the case $h=0$ (see Fig. 12). This behavior is very similar to the one predicted by simulation and presented in Fig. 8, corresponding to the same parameters, after the change of h at t_0.

The evolution of the kink velocity c versus the control parameter is drawn in Fig. 7, where the crosses represent experimental results. Although a small quantitative discrepancy between these experimental results and theoretical predictions (continuous lines) is observed, qualitative behaviors are in good agreement, showing that, in real experimental systems, coupling a chain with a second excited one can speed up the front wave.

E. Modulation of kink velocity

In this section, we propose to propagate a kink in the first chain, while a steady state pattern is present in the second chain. This case was theoretically considered in Sec. IV C.

Parameters of the system are fixed as $a=0.44$, $R_0=3.2\,\mathrm{k}\Omega$, $R'=330\,\mathrm{k}\Omega$, and $h=0.0043$, but the intracoupling resistors R are now different along chain 1: ($R=R_1=3.3\,\mathrm{k}\Omega$) and chain 2 ($R=R_2=150\,\mathrm{k}\Omega$). These values lead to intracoupling coefficient $d_1=0.43$ in chain 1, and $d_2=0.0094$ in chain 2.

Initial conditions for both chains are represented in oscillograms of Figs. 18(a) and 18(b): only the six first cells of chain 1 are in the excited state, while cells of chain 2 exhibit a turing like pattern (see Sec. III). Evolution versus time of these initial conditions shows [see Fig. 18(c)] a propagation of a front wave in chain 1, but whose instantaneous velocity appears not to be constant: the velocity is yet modulated, with transient values successively larger and smaller than the averaged one. Note that the cell voltages in chain 2 quickly reach a steady state pattern [Fig. 18(d)], which corresponds to a periodic rectangular window, and that low (respectively large) values of the kink velocity in chain 1 correspond to the unexcited (excited) cells in chain 2. Figure 18(c) being an experimental counterpart of Fig. 9(a), obtained by numerical calculations, a good agreement between these results is observed.

VI. CONCLUSION

In this paper we have studied the dynamics of two coupled discrete Nagumo chains. Unlike to the case of a single discrete Nagumo chain, where no control exists concerning wave front propagation and its unique velocity, we have shown that the coupling coefficient h is very efficient to discrimine different behaviors of the front waves in both coupled chains. We have intensively studied the case of an homogeneous coupling between the chains, and showed that an initial front wave introduced in chain 1 can either be slowed down, stopped, or ''reversed,'' according to the strength of the coupling, if chain 2 is initially in the vicinity of the unexcited state. On the other hand, the initial front wave in chain 1 can be speeded up, if chain 2 is initially in the vicinity of the excited state. All these properties have been verified in an experimental electrical system composed of two coupled chains of 22 cells. Our experiments confirm, in particular, the possibility of controlling the dynamics of front waves in coupled chains. This may lead to a better understanding of natural phenomena observations in a wide class of systems possessing wave front solutions, in particular in models of coupled neural fiber models [2].

Furthermore, extending this study to two-dimensional coupled systems could offer interesting applications in the field of image processing. In particular, although replication to another lattice of an image initially stored in a first lattice was already studied [30,31], it may be useful to control this replication by means of the interlattices coupling. Moreover, mathematical morphology or contour detection [32] of an initial image would be improved if a coupling coefficient between two lattices could be used to locally control contour propagation, giving either image erosion or dilatation.

ACKNOWLEDGMENTS

This research was supported by the Russian Foundation for Basic Research under Grant No. 00-02-16400. V.I.N would like to thank the Université de Bourgogne for financial support.

[1] J. Murray, *Mathematical Biology* (Springer-Verlag, Berlin, 1989).
[2] A. Scott, *Nonlinear Science: Emergence and Dynamics of Coherent Structures* (Oxford University Press, Oxford, 1998).
[3] R. J. Field and M. Burger, *Oscillations and Traveling Waves in Chemical Systems* (Wiley, New York, 1985).
[4] P. Fife, *Mathematical Aspects of Reacting and Diffusing Systems*, Lecture Notes in Biomathematics Vol. 28 (Springer, Berlin, 1980).
[5] D. Henry, *Geometric Theory of Semilinear Parabolic Equations* (Springer-Verlag, Berlin, 1981).
[6] J. Keener, J. Theor. Biol. **148**, 49 (1991).
[7] M. deCastro, E. Hofer, A. P. Muñuzuri, M. Gómez-Gesteira, G. Plank, I. Schafferhofer, V. Pérez-Muñuzuri, and V. Pérez Villar, Phys. Rev. E **59**, 5962 (1999).
[8] G. Heidemann, M. Bode, and H. G. Purwins, Phys. Lett. A **177**, 225 (1993).
[9] V. P. Villar, IEEE Trans. Circuits Syst. **42**, 665 (1995).
[10] J. Keener, SIAM (Soc. Ind. Appl. Math.) J. Appl. Math. **47**, 556 (1987).
[11] S. Binczak, J. C. Comte, B. Michaux, P. Marquié, and J. M. Bilbault, Electron. Lett. **34**, 1061 (1998).
[12] M. Hiratsuka, T. Aoki, and T. Higuchi, IEEE Trans. Circuits Syst. **46**, 294 (1999).
[13] B. Zinner, SIAM (Soc. Ind. Appl. Math.) J. Appl. Math. **22**, 1016 (1991).
[14] B. Zinner, J. Diff. Eqns. **96**, 1 (1992).
[15] T. Erneux and G. Nicolis, Physica D **67**, 237 (1993).
[16] R. MacKay and J.-A. Sepulchre, Physica D **82**, 243 (1995).
[17] A. Anderson and B. Sleeman, Int. J. Bifurcation Chaos Appl. Sci. Eng. **5**, 63 (1995).
[18] S. N. Chow, J. Mallet-Paret, and E. S. Van Vleck, Int. J. Bifurcation Chaos Appl. Sci. Eng. **6**, 1605 (1996).
[19] P. C. Bressloff and G. Rowlands, Physica D **106**, 255 (1997).
[20] J. C. Comte, P. Marquié, and M. Remoissenet, Phys. Rev. E **60**, 7484 (1999).
[21] J. Keener, Physica D **136**, 1 (2000).
[22] K. Kladko, I. Mitkov, and A. R. Bishop, Phys. Rev. Lett. **84**, 4505 (2000).
[23] J. C. Eilbeck, S. D. Luzader, and A. C. Scott, Bull. Math. Biol. **43**, 389 (1981).
[24] J. Keener, SIAM (Soc. Ind. Appl. Math.) J. Appl. Math. **49**, 210 (1989).
[25] S. Binczak, J. C. Eilbeck, and A. C. Scott, Physica D **148**, 159 (2001).
[26] A. Bose, SIAM (Soc. Ind. Appl. Math.) J. Appl. Math. **55**, 1650 (1995).

[27] P. Tu, *Dynamic Systems. An Introduction with Applications in Economics and Biology* (Springer-Verlag, Berlin, 1994).
[28] V. I. Nekorkin, V. A. Makarov, V. B. Kazantsev, and M. G. Velarde, Physica D **100**, 330 (1997).
[29] V. I. Nekorkin, V. B. Kazantsev, and M. G. Velarde, Phys. Lett. A **236**, 505 (1997).
[30] V. I. Nekorkin, V. B. Kazantsev, M. I. Rabinovich, and M. G. Velarde, Phys. Rev. E **57**, 3344 (1998).
[31] V. I. Nekorkin, V. B. Kazantsev, and M. G. Velarde, Phys. Rev. E **59**, 4515 (1999).
[32] J. Weickert, Anisotropic Diffusion in Image Processing, Vol. ISBN 3-519-02606-6 of ECMI (Teubner-Verlag, Stuttgart, Germany, 1998).